Influence of Vortex Street Structure on the Efficiency of Energy Separation

Andrey I. Aleksyuk[a,b]

[a]*Faculty of Mechanics and Mathematics, Lomonosov Moscow State University, Moscow 119991, Russian Federation*
[b]*Water Problems Institute, Russian Academy of Sciences, Moscow 119333, Russian Federation*

Abstract

Regions with reduced and increased values of total enthalpy are observed in a time-averaged flow behind a bluff body. This energy redistribution takes place both in the vortex formation region and in the developed vortex wake. The present paper focuses on studying the effect of the structure of a vortex street on the intensity of energy redistribution. Two approaches are used. The first one is direct numerical simulation of the flow behind a transversely oscillating cylinder, which is known for a variety of vortex patterns in the wake. The simulations are based on a finite element solution of the Navier-Stokes equations for a compressible perfect viscous gas. The second approach is based on simplified point vortex models for infinite periodic vortex streets, which contain a finite number of vortex chains in equilibrium. It turns out that these simple models make it possible to obtain satisfactory qualitative results, particularly if a more precise approximation of velocity fields in the vortex cores (Rankine vortices) is implemented. It is shown that the effect of energy redistribution significantly depends on the vortex structure, namely the mutual arrangement of the vortices and their intensities. The estimates of the energy separation efficiency in the time-averaged flow are obtained for the general case of an arbitrary number of chains. A more detailed analysis is performed for vortex streets with 2, 3, and 4 vortex chains.

Keywords: energy separation, vortex street, point vortex model, total enthalpy, compressible flow, transversely oscillating cylinder, heat transfer

1. Introduction

For a viscous-gas flow around a cylinder the phenomenon of energy separation is manifested in the appearance of regions with increased and reduced values of total enthalpy in the wake. Such energy redistribution is observed in both instantaneous and time-averaged flow patterns. This problem has been discussed in quite a few studies [1–7]. The interest in the phenomenon of energy separation can be partially explained by the attempts to make energy separation devices more efficient (see, for example, the Ranque-Hilsch vortex tube and the Leontiev tube [8–10]). Another reason for the increased attention to the problem of energy separation in the wake behind bluff bodies is the study of the Eckert-Weise effect, which is manifested in low recovery temperature at the rear part of a thermally insulated cylinder [11].

The lowest values of time-averaged total enthalpy are observed in the vortex formation region and in the developed wake near its centerline [1, 7, 12]. From the energy conservation law, it follows that in a fluid particle the total enthalpy can change due to the action of three mechanisms: the time-variation of pressure at a given point in space; the work of viscous forces; and the heat release due to the thermal conduction effect. The action of all these mechanisms should be taken into account in the vortex formation region; however, in the developed wake it is possible to consider only the first mechanism, related to pressure variation [1, 7].

Since in the formed vortex wake the action of the mechanism related to pressure variation is most significant, the process of energy redistribution can be approximately described by the equation:

$$\frac{Di_0}{Dt} = \frac{1}{\rho}\frac{\partial p}{\partial t},$$

where i_0, p, ρ, and t are total enthalpy, pressure, density, and time, respectively. In [1], the authors explained how particles moving inside and outside the wake form a pattern with reduced values of i_0 near the wake centerline. The main idea is that since the pressure inside the vortices is less than that in the surrounding fluid, i_0 decreases in the fluid particles moving in front of the vortex and increases in the particles moving behind the vortex. Due to the vortex street structure, fluid particles move inside/outside the wake in front of/behind the vortices. The kinematical explanation was suggested based on a modified classical Kármán vortex street model (the Rankine vortices were used instead of potential vortices). It was shown, that the minimum of time-averaged total enthalpy satisfies the equation

$$\overline{i_0} - i_{0\infty} = -\frac{\Gamma_0}{l}(1 + U),$$

Email address: aleksyuk@mech.math.msu.su
(Andrey I. Aleksyuk)

Nomenclature

(u'', v'')	velocity vector in coordinates (x'', y'')
(u', v')	velocity vector in coordinates (x', y')
(u, v)	velocity vector in coordinates (x, y)
(u_1, u_2)	velocity vector in coordinates (x_1, x_2)
(x'', y'')	vector of Cartesian coordinates fixed to moving vortices
(x', y')	vector of Cartesian coordinates, in which the flow at infinity is at rest
(x, y)	vector of Cartesian coordinates of the inertial reference frame, the free stream velocity is $(1, 0)$
(x_1, x_2)	vector of Cartesian coordinates fixed to a cylinder
M	Mach number
$\mathcal{P}, \mathcal{A}, \mathcal{Q}$	contributions of non-stationarity, viscous forces, and thermal conductivity in the total-enthalpy variation rate
Pr	Prandtl number
Re	Reynolds number
$\boldsymbol{n}$	unit normal vector
A	amplitude of cylinder oscillations
C_L	lift coefficient
c_V, c_p	specific heats at constant volume and pressure
d	cylinder diameter
E	efficiency of energy separation
F	normalized (to f_0') frequency of cylinder oscillations
f_0'	vortex shedding frequency for a fixed cylinder
i	unit imaginary number
I_0	normalized total enthalpy
i_0	total enthalpy
l	period of the idealized vortex street along the x axis

N	number of vortex chains forming the idealized vortex street
p	pressure
T	temperature
t	time
U	x-component of vortex velocity in coordinates (x', y')
v_c	transverse velocity of the cylinder
X_{in}, X_{out}, Y	distance from the center of the cylinder to the inlet, outlet, and side boundaries of the corresponding subdomains
y_c	y-coordinate of the cylinder center
z_k	complex coordinates of base potential vortex for chain number k
α_k	normalized circulations Γ_k/Γ
β	ratio lU/Γ
Δ	approximate size of triangular elements of the mesh
γ	specific-heat ratio
Γ_k	circulation of vortices in the chain number k
κ	thermal conductivity
$\boldsymbol{\tau}$	viscous stress tensor
μ	viscosity coefficient
ω	vorticity
ρ	density
ε	energy
$(\cdot)_{,i}$	coordinate derivatives, $i = 1, 2$ corresponds to x, y
$(\cdot)_{,t}$	time derivatives
0	stagnation (or total) parameters
∞	free-stream parameters
$'$	dimensional parameters
$*$	transposition
$\overline{(\cdot)}$	time-averaged value

where $i_{0\infty}$ is the total enthalpy in the free stream, Γ_0 is the absolute value of the vortex circulation, l is the period of the vortex street along the x-axis, $1 + U$ is the velocity of vortices in the reference frame fixed to the cylinder, and the bar signifies time averaging.

The analysis of a time-averaged flow in [7] indicated that the main reason for the variation of $\overline{i_0}$ is the appearance of a negative correlation $\overline{\boldsymbol{u}' \cdot \nabla i_0'}$ induced by the pressure variation due to the nonlinear term in the energy conservation law. Here, $\boldsymbol{u}$ is the velocity vector, $\boldsymbol{u}' = \boldsymbol{u} - \overline{\boldsymbol{u}}$, and $i_0' = i_0 - \overline{i_0}$.

The present study focuses on the influence of the vor-

tex wake structure on the total-enthalpy distribution. Developing the kinematical-explanation approach described above, we apply both direct numerical simulations and consider various equilibrium configurations of simplified point vortex models for several vortex street structures.

We consider the problem of forced transverse oscillations of a circular cylinder in a uniform flow based on the direct numerical solution of Navier-Stokes equations by the finite-element method (Section 2). This problem is known for a variety of flow regimes in the wake. The diagram of wake patterns can be found in [13, 14]. Among others it contains 2S, P, 2P, and P+S modes. Here, the notation of each mode describes how the cylinder sheds vortices per one cycle of the oscillations (S and P mean a single vortex and a pair of vortices respectively). In Section 3.1, we consider flows at Re = 500, M = 0.4, Pr = 0.72 and different frequencies and amplitudes of forced oscillations to demonstrate the influence of the vortex street structure on the time-averaged total enthalpy distribution.

In Section 3.2, several equilibrium configurations of point vortex models are considered to estimate the influence of vortex structure on the energy separation efficiency. The predictions based on these models are in good agreement with the computation results, given the limitations discussed in Section 3.2. We restrict our consideration to vortex streets combined of 2, 3, and 4 infinite chains of potential vortices. For the details of the properties of such models see [15–19].

2. Problem formulation and numerical method

In the inertial reference frame (x, y), the circular cylinder oscillates transversely in a uniform flow. The transverse displacement of the cylinder is given by the expression $y_c(t) = A \sin(2\pi f t)$; here, A and f are amplitude and frequency. The fluid surrounding the cylinder is described by the model of a viscous perfect gas with constant specific heats, viscosity, and thermal conductivity.

The problem is formulated in the Cartesian coordinate system (x_1, x_2) fixed to the circular cylinder, with the origin located at its center (see Fig. 5a). The Navier–Stokes equations governing the compressible fluid flow are solved in primitive variables $\boldsymbol{Y}(\boldsymbol{x}, t) = (p, u_1, u_2, T)^*$; here, p, $\boldsymbol{u} = (u_1, u_2)^*$ and T are the dimensionless pressure, velocity vector, and temperature; $\boldsymbol{x} = (x_1, x_2)^*$; and * is transposition. After the transition from the conservative variables the Navier–Stokes equations can be written in the following form

$$\boldsymbol{A}_0 \boldsymbol{Y}_{,t} + \boldsymbol{A}_i \boldsymbol{Y}_{,i} = \left(\boldsymbol{K}_{ij} \boldsymbol{Y}_{,j} - \boldsymbol{P}_i\right)_{,i} + \boldsymbol{R}. \tag{1}$$

The explicit expressions for matrices $\boldsymbol{A}_0$, $\boldsymbol{A}_i$, $\boldsymbol{K}_{ij}$ and vectors $\boldsymbol{P}_i$, $\boldsymbol{R}$ $(i, j = 1, 2)$ are given in Appendix A. The last vector on the right-hand side arises due to the use of the non-inertial reference frame. The repeated indices imply summation, and the short notation for the derivatives is used $(\cdot)_{,t} = \partial(\cdot)/\partial t$, $(\cdot)_{,1} = \partial(\cdot)/\partial x_1$, $(\cdot)_{,2} = \partial(\cdot)/\partial x_2$.

Domain	Δ	X_{in}	X_{out}	Y
Boundary layer	0.0005	-	-	-
Near wake	0.025	1.5	26	5
Middle wake	0.05	3	40	8
Far wake	0.25	6	80	16
Entire domain	2.5	200	400	200

Table 1: Parameters of the mesh. The number of nodes is $N_v = 930930$. The number of elements is $N_e = 1861860$. Δ is the approximate size of triangular elements of the mesh, X_{in}, X_{out}, and Y are the distances from the center of the cylinder to the inlet, outlet, and side boundaries of the corresponding subdomains.

All quantities are dimensionless; nondimensionalization is performed using the following formulas (here, dimensional quantities are denoted by primes)

$$t = \frac{u_\infty t'}{d}, \ \ \boldsymbol{x} = \frac{\boldsymbol{x}'}{d}, \ \ p = \frac{p'}{\rho_\infty u_\infty^2}, \ \ \boldsymbol{u} = \frac{\boldsymbol{u}'}{u_\infty}, \ \ T = \frac{c_V T'}{u_\infty^2}.$$

The Reynolds Re, Prandtl Pr, and Mach M numbers are defined by the following formulas:

$$\text{Re} = \frac{\rho_\infty u_\infty d}{\mu}, \ \ \text{Pr} = \frac{\mu c_p}{\kappa}, \ \ \text{M} = \frac{u_\infty}{c_\infty}.$$

Here, d is the diameter of the cylinder; ρ_∞, p_∞, u_∞ are the free-stream density, pressure, and velocity; κ, μ are the thermal conduction and viscosity coefficients; c_V, c_p are the specific heats at constant volume and pressure; $c_\infty = \sqrt{\gamma p_\infty / \rho_\infty}$ is the sonic velocity in the free stream; and $\gamma = 1.4$ is the specific heat ratio. Amplitude A and frequency f of cylinder oscillations are also dimensionless: $A = A'/d$, $f = f'd/u_\infty$. In what follows, we will use the dimensionless parameter $F = f'/f_0'$ instead of f; here, f_0' is the vortex shedding frequency for a fixed cylinder.

In the non-inertial reference frame, the following boundary conditions are assumed. On the cylinder surface, the velocity no-slip $\boldsymbol{u} = (0, 0)$ and adiabatic-wall $\nabla T \cdot \boldsymbol{n} = 0$ conditions are prescribed (here, $\boldsymbol{n}$ is a unit normal vector). At infinity, $\boldsymbol{u} = (1, -v_c)$, $p = 1/(\gamma \text{M}^2)$, and $T = 1/[\gamma(\gamma - 1)\text{M}^2]$, where $v_c = y_{c,t}$.

For numerical solution of this problem, we use the Galerkin least-squares (GLS) finite-element method on unstructured triangular meshes. The algorithms used have been successfully applied to the simulation of several problems of compressible and incompressible viscous flows around bodies (for details, see [7, 20, 21]).

Table 1 shows the parameters of the mesh used, which is divided into several nested subdomains with different step sizes. The results of algorithm testing for similar regimes of the flow can be found in [7]. In this study, we enlarged the region of 'Near wake' along and across the flow, since here we consider wider wakes due to cylinder oscillations and also because we are interested in the development of the wakes at longer distances downstream.

The numerical results in following section are restricted to Re = 500. This Reynolds number was chosen to reduce
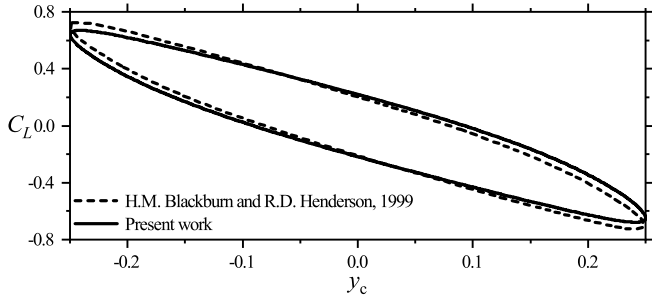
Fig. 1: The dependence of lift coefficient C_L on cylinder displacement y_c for limit cycle at $F = 0.89$, $A = 0.25$, Re = 500. The dashed line is data from [22] and the solid line is the present results (M = 0.1 and Pr = 0.72).

the viscous diffusion effect and to obtain periodic regimes of a two-dimensional compressible flow ($M = 0.4$) around a fixed cylinder. In [7] (Figs. 10-12) it was shown that at Re $\geq$ 500 the effect of the Reynolds number is not as pronounced as at Re $<$ 500. It should be noted, that the real flow at Re = 500 is three-dimensional and turbulent. However, we believe that the described mathematical model takes into account enough underlying physics to qualitatively demonstrate the influence of a vortex street on the efficiency of energy separation (Section 3.1) and to study the adequacy of simplified point vortex models predicting the efficiency of this process in a developed wake (Section 3.2). In [22] the incompressible two-dimensional flow past an oscillating cylinder at Re = 500 and $A = 0.25$ was studied. Figure 1 demonstrates the agreement in the lift coefficient $C_L(y_c)$ with these results at Re = 500, $F = 0.89$, $A = 0.25$. Figure 2 shows the transition between two vortex shedding regimes at Re = 200 and $F = 1.01$: 2S mode at $A = 0.6$ and P+S mode at $A = 0.8$. These results are in agreement with the data in [14], where it was shown that the boundary amplitude A between two modes is approximately 0.7 (see Fig. 5a and 7 in [14]).

3. Energy redistribution for different wake patterns

Total enthalpy i_0 is considered in the coordinates $(x, y) = (x_1, x_2 + y_c)$ ($u = u_1$, $v = u_2 + v_c$): the cylinder has zero x-component of the velocity and performs only transverse oscillations. We define normalized total enthalpy I_0 by the expression

$$I_0(x, y, t) = \frac{i_0 - i_{0\infty}}{i_{0\infty}}, \quad i_0(x, y, t) = \gamma T + 0.5 \left(u^2 + v^2 \right), \quad (2)$$

and introduce the time-averaged flow parameters denoted with the bar: $\overline{f}(x, y) = (t_2 - t_1)^{-1} \int_{t_1}^{t_2} f(x, y, t) dt$, for some function $f(x, y, t)$ and long enough time interval $t_2 - t_1$, excluding initial stages of flow development. In the present work, time-averaged distributions were obtained by averaging over the intervals not less than 215 (approximately

(a) $A = 0.6$

(b) $A = 0.8$

(c) Color map for ω
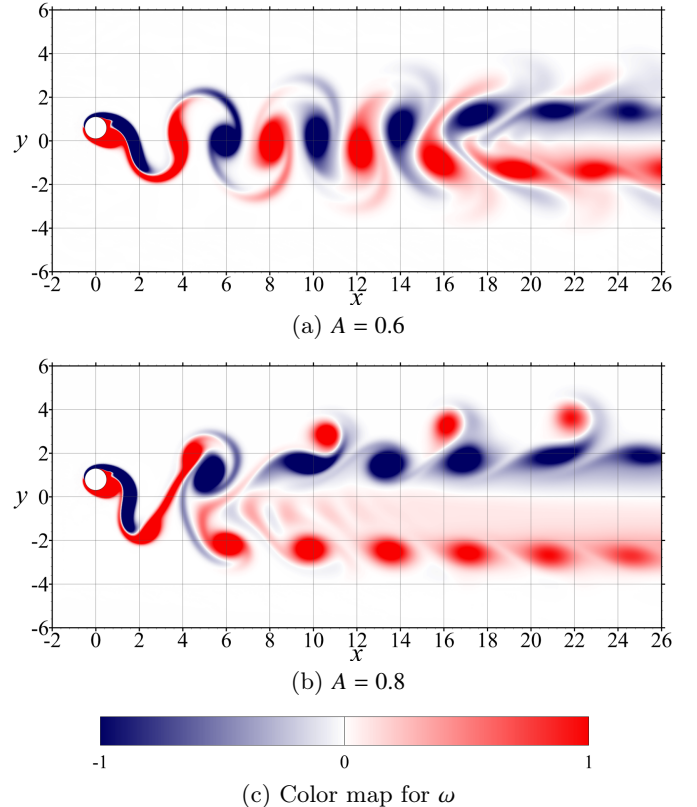
Fig. 2: The transition from 2S (a) to P+S (b) shedding mode in the wake at $F = 1.01$, Re = 200, M = 0.1 and Pr = 0.72. Limit values on the color map are not the maximum and minimum of function ω: function values greater than the upper limit (or less than the lower limit) are filled with one color corresponding to this limit. (For the interpretation of the references to color in this figure legend, the reader is referred to the web version of this article.)

48 vortex shedding periods for a fixed cylinder) with the time step being equal to 0.2. The minimum value of the normalized total enthalpy in the time-averaged flow is considered as the indicator of energy separation efficiency

$$E(\Omega) = \left| \min_{(x,y) \in \Omega} \overline{I_0}(x, y) \right|.$$

The value of E depends on the flow subregion Ω under consideration, for example, it could be the vortex formation region or some parts of the developed wake.

The equation for the total-enthalpy variation in the coordinates (x, y) can be written as follows:

$$\frac{Di_0}{Dt} = \underbrace{\frac{1}{\rho} \frac{\partial p}{\partial t}}_{\mathcal{P}} + \underbrace{\frac{1}{\rho \text{Re}} \nabla \cdot (\boldsymbol{\tau} \cdot \boldsymbol{v})}_{\mathcal{A}} + \underbrace{\frac{1}{\rho \text{RePr}} \nabla^2 T}_{Q}. \quad (3)$$

Here, $D/Dt = \partial/\partial t + \boldsymbol{v} \cdot \nabla$ is the material derivative and $\boldsymbol{v} = (u, v)^*$. The description of the contribution of each term in the equation for a fixed cylinder can be found in [7]. The reason for energy redistribution in the developed wake is related to the nonlinearity in the left-hand side of Eq. (3) and to the action of term $\mathcal{P}$, whereas the

(a) Fixed cylinder

(b) $A = 1$, $F = 0.5$

(c) $A = 0.25$, $F = 0.7$

(d) $A = 0.75$, $F = 0.7$

(e) $A = 0.5$, $F = 1$

(f) $A = 1$, $F = 1$

(g) Color map for $\overline{I_0}$
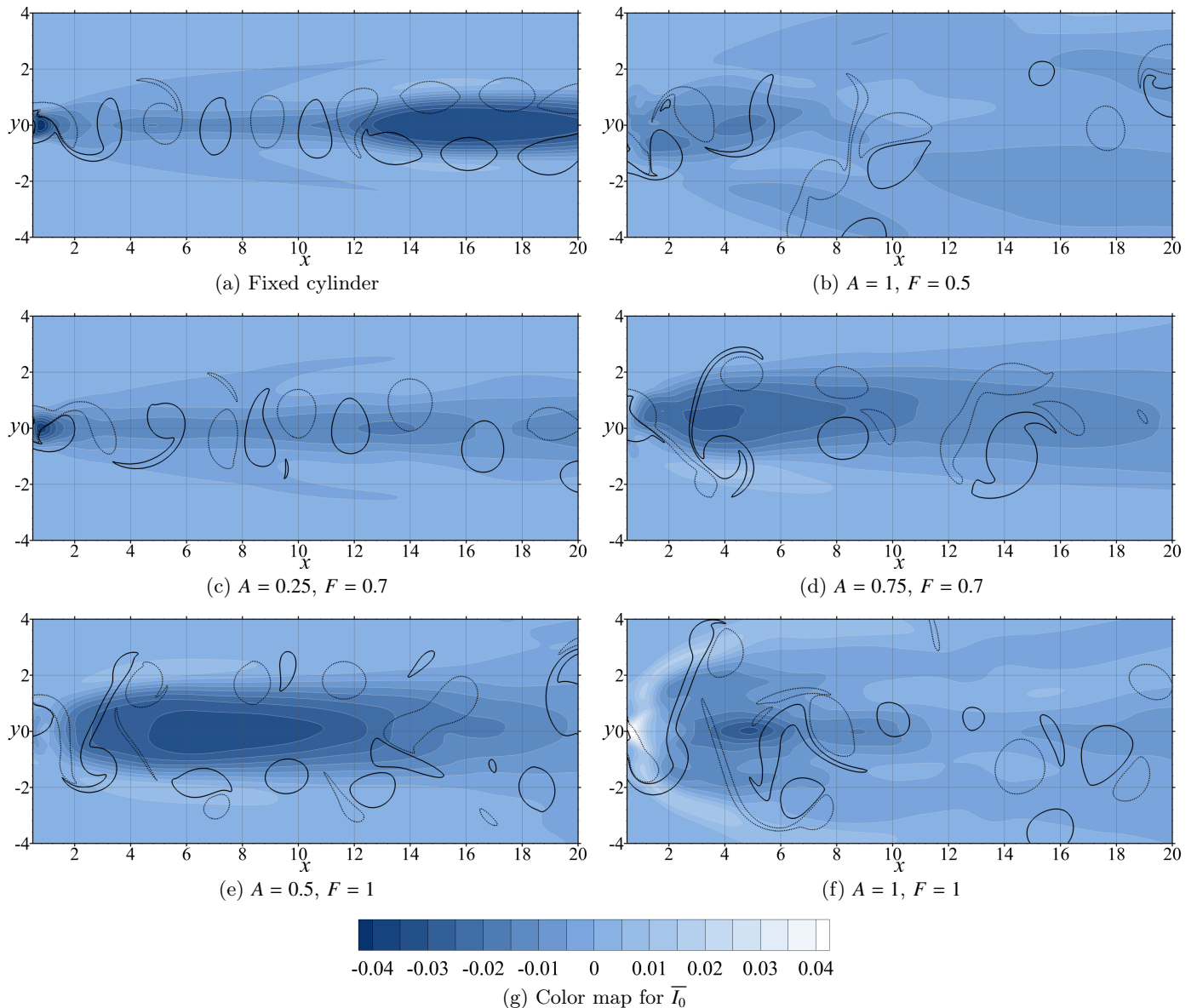
Fig. 3: The influence of the wake structure on the time-averaged total enthalpy distribution $\overline{I_0}$ at Re = 500, M = 0.4 and Pr = 0.72. Here, solid and dashed lines correspond to positive and negative constant values of vorticity $\omega = \pm 0.5$ at an arbitrary instant of time. (For the interpretation of the references to color in this figure legend, the reader is referred to the web version of this article.)

other terms $(\mathcal{A}, \mathcal{Q})$ are negligible in the wake [1, 4, 7]. The pressure fields in the wake are mainly determined by vortex dynamics. That is why we are interested in studying the effect of vortex street structures on the energy redistribution. This section demonstrates the influence of the wake pattern on the efficiency of energy separation based on both direct numerical simulation and simplified point vortex modeling of the wake.

3.1. Total-enthalpy distribution for a transversely oscillating cylinder

Transverse oscillations of the cylinder cause energy transfer between the flow and the cylinder. For a period

of time $t_1 \le t \le t_2$, it can be expressed by the coefficient

$$C_E = \int_{t_1}^{t_2} C_L v_c dt. \tag{4}$$

Equation (4) expresses the work done by the fluid. If $C_E < 0$, energy transfers from the cylinder to the fluid, and vice versa. In the first case ($C_E < 0$), the shedding vortices tend to suppress the cylinder oscillations, and in the second case ($C_E > 0$) they tend to strengthen these oscillations. In this section, we consider the regimes with $C_E < 0$.

In Fig. 3 we present the averaged distribution of total enthalpy for different frequencies F and amplitudes A, and also the isolines $\omega = \pm$const for a certain instant of

5

time. The wake structure turns out to be mostly irregular; however, in most cases the time-averaged flow fields have reflective symmetry with respect to the wake centerline $y = 0$. The loss of symmetry is clearly observed for $A = 1, F = 0.5$ and $A = 0.75, F = 0.7$ (Fig. 3b, d). At $A = 0.75$ and $F = 0.7$ (Fig. 3d), the vortices are shed in accordance with the P+S scheme: a single vortex on one side and a pair of vortices on the other. Therefore, as a result of averaging, the region of reduced total enthalpy is shifted away from the centerline. At $A = 1$ and $F = 0.5$ (Fig. 3b), the widest region of lowered $\overline{I_0}$ is observed among the considered regimes. The vortex dynamics is complicated and it is difficult to construct the pattern in this case. Most of the time, the vortices are shed in pairs, but their trajectories are complex and differ from one cycle to another.

From Fig. 3, it is clear that when the vortices of opposite signs move with lesser transverse distance, smaller values of E are attained (in the general case, it is not true, see Section 3.2). For example, see Figs. 3a, c, e for $x \lesssim 12$ and $x \gtrsim 12$; and Figs. 3d, f for $x \lesssim 6$ and $x \gtrsim 6$. Another finding is the following: if the positive vortex moves above (at a greater y value than) the negative one, then the value of $\overline{I_0}$ between them is positive, and vice versa. Such thin bands of positive $\overline{I_0}$ are clear in Figs. 3d, e, f for the regions of motion of some vortex pairs. These features can be explained using the simplified point vortex models; see Section 3.2.

Particular attention should be paid to the effect shown in Fig. 3a: after the change in the wake structure the minimum value of the total enthalpy ($E \approx 0.034$) becomes closer to its values in the formation region ($E \approx 0.044$), while the region of reduced values is much larger. This effect is attributable to changing the vortex structure. In the next section, it will be considered in more detail.

As the amplitude of oscillations becomes high enough, the formation region is no longer the region with minimal values of $\overline{I_0}$. Moreover, in this region much greater values of $\overline{I_0}$ can be attained ($\max \overline{I_0} \approx 0.045$ for $A = 1$ and $F = 1$, see Fig. 3f). For a fixed cylinder, on the contrary, the smallest values are usually observed in this region. As shown numerically for a fixed cylinder [7], the region responsible for the decrease in $\overline{I_0}$ in the vortex formation zone does not affect the decrease of $\overline{I_0}$ in the developed vortex street. It is related to the formation of recirculation zones near the body in the time-averaged flow fields, where the lowest values of $\overline{I_0}$ are observed; see, for example Fig. 4a. If the oscillation amplitude A is not high, there are still some recirculation zones in the time-averaged flow in which one can find the minimum of $\overline{I_0}$ (Fig. 4b). However, when A is high enough the time-averaged recirculation zones disappear (Fig. 4c) and the mechanisms [7] of reduction of $\overline{I_0}$ in the formation region are absent. Thus, the minimal values of $\overline{I_0}$ are not observed in the formation region in Figs. 3b, d-f and Fig. 4c. Another consequence of this is that the distribution of $\overline{I_0}$ in the formation region has a greater impact on $\overline{I_0}$ in the developed wake (in terms of analysis of the time-averaged mechanisms [7]).

(a) Fixed cylinder

(b) $A = 0.25$, $F = 0.7$

(c) $A = 0.75$, $F = 0.7$

-0.04 -0.03 -0.02 -0.01   0   0.01 0.02 0.03 0.04

(d) Color map for $\overline{I_0}$
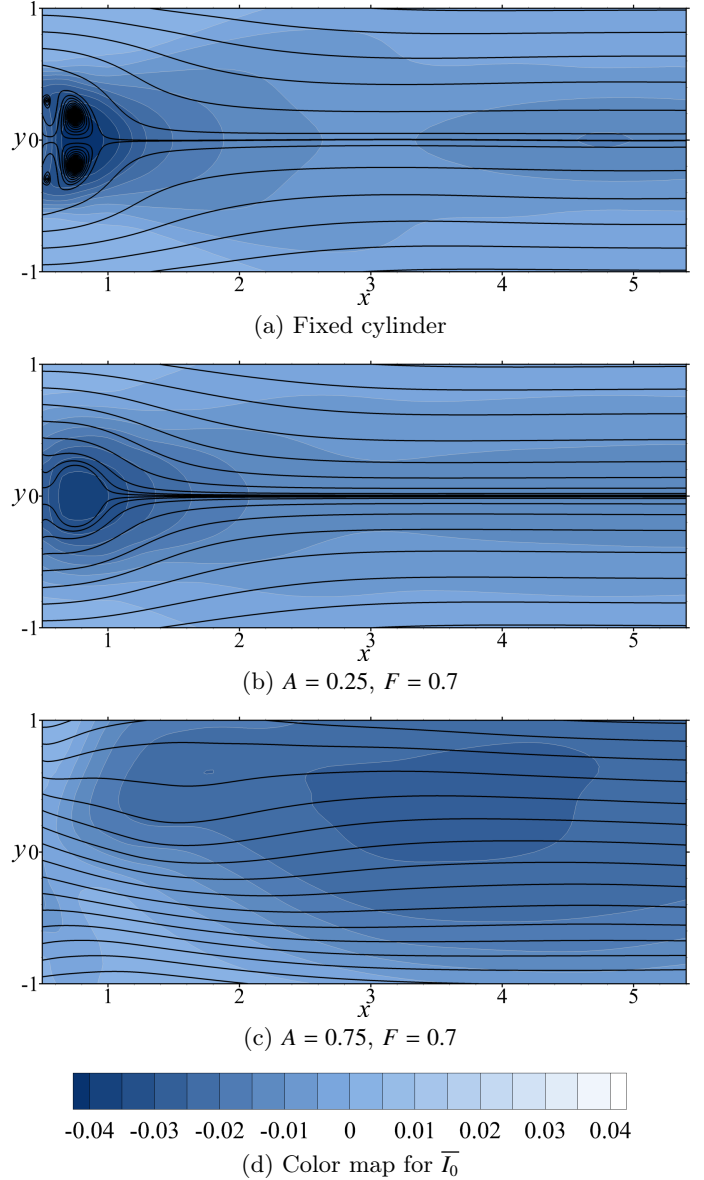
Fig. 4: Time-averaged total enthalpy distribution $\overline{I_0}$ and streamlines at Re = 500, M = 0.4 and Pr = 0.72. (For the interpretation of the references to color in this figure legend, the reader is referred to the web version of this article.)

Among the regimes considered in Fig. 3, in the developed wake the value of E has its maximum for a fixed cylinder, $E \approx 0.035$. With the increase in amplitude A at $F = 1$, the efficiency decreases ($E \approx 0.033$ at $A = 0.5$ and $E \approx 0.031$ at $A = 1$), but for $A = 0.5$ the area of the region of reduced $\overline{I_0}$ is maximal. The same behavior can be observed for $F = 0.7$ ($E \approx 0.039$ at $A = 0.25$ and $E \approx 0.026$ at $A = 0.75$). It should be noted that the data presented are not sufficient to make definitive conclusions on the influence of A or F.
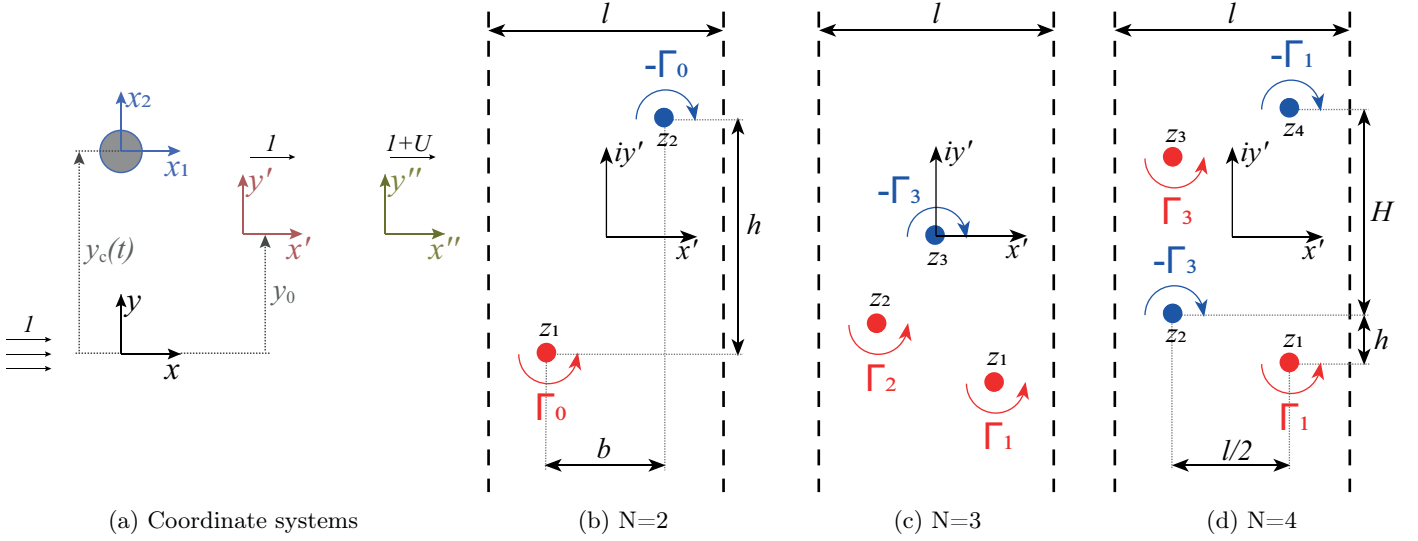
Fig. 5: Schemes for different coordinate systems (a) and for one period of the considered point vortex models with $N = 2$, 3 and 4 (b-d).

3.2. Estimates of energy separation efficiency based on the point vortex models

Since the main mechanism of energy separation in the developed wake is the time variation of pressure, it is possible to estimate the effect of the vortex wake structure on the energy separation efficiency using a simplified model of a vortex wake formed by potential vortices. A similar analysis was carried out earlier for the classical staggered Kármán street [1]. To be complete, we repeat the assumptions required for calculating $\overline{I_0}$.

The flow is assumed to be inviscid and non-heat-conducting. It is further assumed that the wake has a longitudinal period l; vortices in the wake move with constant velocity $1 + U$ along the x-axis (velocity at infinity is 1 in dimensionless variables), which is greater than zero and less than 1, so $-1 < U < 0$. We introduce the following coordinate systems (Fig. 5a).

O1: The flow at infinity is at rest, i.e.

$x' = x - t$, $y' = y - y_0$, where y_0 is constant;
$u'(x', y', t) = u(x' + t, y' + y_0, t) - 1$,
$v'(x', y', t) = v(x' + t, y' + y_0, t)$.

O2: The flow in the wake is stationary, i.e.

$x'' = x - (U + 1)t$, $y'' = y - y_0$;
$u''(x'', y'') = u(x'' + Ut + t, y'' + y_0, t) - (U + 1)$,
$v''(x'', y'') = v(x'' + Ut + t, y'' + y_0, t)$.

In O2 the flow is stationary, so the total enthalpy $i''_0 = \gamma T + 0.5(u''^2 + v''^2)$ is constant along streamlines; we assume that this constant is the same for any streamline (for example, for isentropic irrotational flow). Thus, using the value of i''_0 at infinity,

$$i''_0(x'', y'') = \gamma T + 0.5(u''^2 + v''^2) = \gamma T_\infty + 0.5U^2. \quad (5)$$

Here, T_∞ is the dimensionless temperature at infinity, and $\gamma T_\infty = i_{0\infty} - 0.5$. Excluding temperature T from Eqs. (2) and (5), one can obtain the following expression.

$$i_0(x, y, t) - i_{0\infty} = (1 + U)(u - 1).$$

For theoretical estimations in the present section purely periodic flows are considered, hence, in the definition of time-averaging (given in the beginning of Section 3) $t_2 - t_1$ equals one time period. Moreover, time-averaging coincides with spatial averaging along the x axis and

$$\overline{u}(y) = \frac{1}{t_2 - t_1} \int_{t_1}^{t_2} u(x, y, t)dt = U + 1 + \frac{1}{l} \int_{\xi}^{\xi+l} u''(\xi, y - y_0)d\xi,$$

$$\overline{u'}(y') = \frac{1}{t'_2 - t'_1} \int_{t'_1}^{t'_2} u'(x', y', t)dt = U + \frac{1}{l} \int_{\xi}^{\xi+l} u''(\xi, y')d\xi.$$

Here, $(U + 1)(t_2 - t_1) = U(t'_2 - t'_1) = l$. Hence,

$$\overline{I_0}(y) = \frac{(1 + U)}{i_{0\infty}} \overline{u'}(y - y_0). \quad (6)$$

The efficiency of energy separation equals $E = (1 + U)|\overline{u'}_{min}|/i_{0\infty}$, where $\overline{u'}_{min} = \min_{y'} \overline{u'}(y')$.

Thus, to estimate the energy separation efficiency, it is necessary to construct the velocity fields for different configurations of a periodic vortex wake. For this purpose, we use the point vortex models of the wake, which were studied previously in numerous works; see, for example, [15–19].

It is worth giving a few comments on the applicability of these models. The point vortex models do not reflect the

shape of the vortices and predict incorrect velocity distribution in the vortex cores (additional remarks on it will be made in the next subsection). In addition, the considered model does not reproduce a variation in the mutual arrangement of the vortices. Partially it could be taken into account by considering non-equilibrium regimes; see, for example, [17]. Not all of the considered configurations are stable and can be realized in nature [15, 17, 18]. Moreover, this model assumes that the fluid is incompressible, and the compressibility effects could change some parameters of the flow. For example, in [23] one can find theoretical estimates of variations in U for a weakly compressible fluid. Finally, viscous diffusion is absent in the point-vortex model. Nevertheless, these models provide a very convenient tool for understanding the general ways of increasing/decreasing the energy separation effect by changing the intensity and mutual arrangements of vortices.

In a general case, let there be a periodic vortex wake with a longitudinal period l, which is formed by N infinite chains of vortices, see Fig. 5b-d. In each chain, we denote the complex-valued coordinates of the vortices defining the mutual position of the chains by $z_k = x'_k + iy'_k$, $k = 1, ..., N$. The velocity field created by a system of point vortices is given by

$$u' - iv' = \sum_{k=1}^{N} \frac{\Gamma_k}{2li} \cot \frac{\pi}{l}(z - z_k).$$

Using this equation, one can obtain the expression for $\overline{u'}$:

$$\overline{u'} = -\sum_{k=1}^{N} \frac{\Gamma_k}{2l} \operatorname{sgn}(y' - y'_k). \quad (7)$$

The velocity of each vortex z_α is determined from the relation

$$u'_\alpha - iv'_\alpha = \sum_{k=1, k\neq\alpha}^{N} \frac{\Gamma_k}{2li} \cot \frac{\pi}{l}(z_\alpha - z_k). \quad (8)$$

For equilibrium solutions, the positions of the vortices relative to each other do not change, so

$$u'_\alpha = U, \quad v'_\alpha = 0, \quad \sum_{k=1}^{N} \Gamma_k = 0. \quad (9)$$

Here, we use the fact that the motion occurs along the x-axis with velocity $U < 0$. The last relation in Eqs. (9) is obtained from the first two conditions after multiplying by Γ_α Eq. (8) and summing over index α.

We introduce the following parameters, which characterize the flow: $\beta = lU/\Gamma < 0$ and $\alpha_k = \Gamma_k/\Gamma$, $\Gamma = |\Gamma_1| + |\Gamma_2| + ... + |\Gamma_N|$, $\alpha_1 + \alpha_2 + ... + \alpha_N = 0$, $k = 1, ..., N$. If α_k and β are given, one can obtain a solution (or solutions) of Eqs. (8) and (9), which defines certain mutual arrangement of vortices up to scaling l. From Eqs. (6) and (7) we have

$$\overline{I_0} = -\frac{\Gamma}{2li_{0\infty}}(1 + \beta\frac{\Gamma}{l}) \sum_{k=1, k\neq m}^{N} \alpha_k[\operatorname{sgn}(y' - y'_k) - \operatorname{sgn}(y' - y'_m)]$$

for any $m = 1, 2, ..., N$. For any fixed mutual arrangement of vortices up to scaling l, with given α_k and β, the maximum of E (the minimum of $\overline{I_0}$) is attained for $\beta\Gamma/l = -0.5$ (since positive factor $(\Gamma/l)(1 + \beta\Gamma/l)$ is maximal), i.e.

$$E = \frac{\Gamma}{4li_{0\infty}} \max_{y'} \left\{ \sum_{k=1, k\neq m}^{N} \alpha_k[\operatorname{sgn}(y' - y'_k) - \operatorname{sgn}(y' - y'_m)] \right\}.$$

Since $\sum_{k=1}^{N} |\alpha_k| = 1$ and the absolute value of the expression in square brackets is less than 2, the following estimate is valid

$$E \leq \frac{\Gamma}{2li_{0\infty}} \min_k(1 - |\alpha_k|) \leq \frac{\Gamma(N-1)}{2li_{0\infty}N} = -\frac{N-1}{4\beta i_{0\infty}N}. \quad (10)$$

Furthermore, since $i_{0\infty} > 0.5$ (in our calculations $M = 0.4$ and $i_{0\infty} = 129/8$), $E \leq \Gamma(N-1)/(lN)$.

We can use Rankine vortices instead of potential ones to better approximate the velocity field in the vortex cores. Despite the fact that the flow inside vortex cores is no longer irrotational, we still assume that Eq. (6) is approximately valid. It is true if $\int_\xi^{\xi+l} i''_0(\xi, y')d\xi/l \approx i''_{0\infty}$ (for example, if $i''_0(x', y') = i''_{0\infty}$, as was assumed above). Thus, one should modify only the expression for $\overline{u'}$, instead of Eq. (7),

$$\overline{u'} = \sum_{k=1}^{N} \frac{\Gamma_k}{2l} \operatorname{sgn}(y' - y'_k) \left[\theta_k(y')\frac{2}{\pi} \arctan \sqrt{\left(\frac{R_k}{y' - y'_k}\right)^2 - 1} - 1\right]$$
$$- \sum_{k=1}^{N} \frac{\Gamma_k}{\pi l} \theta_k(y')\frac{y' - y'_k}{R_k} \sqrt{1 - \left(\frac{y' - y'_k}{R_k}\right)^2}. \quad (11)$$

Here, R_k is the radius of the core of vortices in k-chain and $\theta_k(y')$ equals 1 if $(y' - y'_k)^2 < R_k^2$, otherwise it is zero. This function is continuous, unlike the case of potential vortices for which it is piece-wise constant.

Below, we consider three cases shown in Fig. 5b-d: classical symmetric and staggered Kármán streets with $N = 2$, equilibrium configurations of three vortices with $N = 3$, and a symmetric wake with $N = 4$.

3.2.1. N=2

Let us introduce additional notations for this subsection (Fig. 5b): $\Gamma_1 = -\Gamma_2 = \Gamma_0 = 0.5\Gamma > 0$ and $z_2 - z_1 = b + ih$, where $b, h \geq 0$. For symmetric ($b = 0$) and staggered ($b = 0.5l$) Kármán streets, one can obtain

$$E = \begin{cases} \frac{\Gamma}{2li_{0\infty}} \left(1 - \frac{\Gamma}{4l} \coth \frac{\pi h}{l}\right), & b = 0, \\ \frac{\Gamma}{2li_{0\infty}} \left(1 - \frac{\Gamma}{4l} \tanh \frac{\pi h}{l}\right), & b = 0.5l, \end{cases} \quad (12)$$

due to the fact that $\overline{u'}_{min} = -\Gamma_0/l$ at $y'_1 < y' < y'_2$ and $U = -(\Gamma_0/2l)\coth(\pi h/l)$ or $U = -(\Gamma_0/2l)\tanh(\pi h/l)$ for a symmetric or a staggered Kármán street. In terms of the previous analysis, $\alpha_1 = -\alpha_2 = 0.5$ and $\beta = -0.25\coth(\pi h/l)$ or $\beta = -0.25\tanh(\pi h/l)$ for a symmetric or a staggered Kármán street.

8

Let us now consider the effect of parameters in Eq. (12) on the energy separation efficiency. When other parameters are fixed, the optimal value of Γ/l is $2\tanh(\pi h/l)$ $(b = 0)$ or $2\coth(\pi h/l)$ $(b = 0.5l)$. The smaller the transverse distance between vortices h, the more intense is the energy separation for a staggered Kármán street, with the maximum effect $E = \Gamma/(2li_{0\infty})$ being attained at $h = 0$. For a symmetric wake, on the contrary, as the transverse distance decreases, the intensity decreases. The maximum efficiency (at $h \to +\infty$) is equal to the minimum for a staggered Kármán street: $E = \Gamma/(2li_{0\infty})[1 - \Gamma/(4l)]$.

A vivid example of the effect of a staggered wake structure with $N = 2$ on E is clearly seen in Fig. 3a. Upstream and downstream from $x \approx 12$, the wake structure is different and E is significantly different. To estimate the parameters, we choose two vortices upstream ($6 < x < 10$) and two vortices downstream ($16 < x < 18$). Thus, upstream $l \approx 3.7$, $h \approx 0.29$ ($\Gamma_0 \approx 3.8$), and downstream $l \approx 2.8$, $h \approx 2.12$ ($\Gamma_0 \approx 2.86$). The calculations of E using Eq. (12) give ($i_{0\infty} = 129/8$)

Upstream: $E = 0.056$ ($U = -0.12$, $\overline{u'}_{\min} = -1.03$),

Downstream: $E = 0.032$ ($U = -0.50$, $\overline{u'}_{\min} = -1.02$).

The result is that the efficiency decreases, which contradicts the direct numerical simulations in Fig. 3a. This can be explained by the following. The point vortex model does not describe correctly the velocity fields near the vortex cores. When the vortices in the upstream part of the wake are located near the centerline, this drawback of the model does not allow one to achieve qualitatively correct values of $\overline{u'}_{\min}$ and, hence, correct values of E. However, for the downstream part of the flow it is not a problem. Indeed, from the numerical results, we have:

Upstream: $E = 0.013$ ($U = -0.2$, $\overline{u'}_{\min} = -0.3$),

Downstream: $E = 0.034$ ($U = -0.4$, $\overline{u'}_{\min} = -0.97$).

We can see that the main discrepancy with the model is in $\overline{u'}_{\min}$ upstream. Downstream parameters are in good agreement. It is possible to obtain much better agreement in the upstream wake if we replace the point vortices in the model by Rankine vortices (Eq. (11)), giving $E \approx 0.020$, $\overline{u'}_{\min} \approx -0.38$ ($U = -0.12$). An approximate value for the vortex core radius was taken equal to 0.5 in accordance with the numerical results.

As shown above, when the Rankine vortices are used to approximate the velocity field it is possible to obtain a general expression for $\overline{I_0}$ and efficiency E. When considering Eq. (11) with $N = 2$, one can see that if $h/2$ is greater than the vortex core radius R, then E is the same as for the potential vortices and increases with decrease in h. However, if $h < 2R$ the value of E decreases to zero with $h \to 0$. Thus, one can expect that in a real flow for fixed Γ_0, l, R the efficiency of energy separation E has its maximum when h is close to $2R$.

Let us also compare the numerical results for this case with the maximal possible efficiency predicted by the model (Eq. (10)): $E_{\max} \approx 0.032$ upstream and downstream (since Γ/l is almost equal). This value is close to E in the real flow downstream, because the vortex cores have a smaller impact on the time-averaged velocity field.

This comparison shows that the point vortex models make it possible to estimate values of E if the vortex cores are located far enough from the region of minimum values of $\overline{I_0}$. In case they are not, one can improve the estimate by the replacement of point vortices with Rankine vortices. When vortex cores are less involved in the formation of the time-averaged velocity field inside the region with minimum values of $\overline{I_0}$, the efficiency of energy separation is greater.

As noted above, for a symmetric vortex street E increases with h. That is what we observed in Section 3.1, for example, in Fig. 3d. One can approximate the vortex wake fragment in Fig. 3d at $4 < x < 9$ by a symmetric vortex street: from averaging using four vortices $l \approx 3.9$, $h \approx 2.5$ and $\Gamma_0 \approx 4.2$. From the model (Eq. (12)) $E \approx 0.03$ which is in qualitative agreement with the calculations $E \approx 0.026$.

3.2.2. $N=3$

We assume that $\Gamma_1, \Gamma_2 \geq 0$, $\Gamma_1 + \Gamma_2 = -\Gamma_3 = \Gamma_0 = 0.5\Gamma > 0$, and $\alpha_0 = \Gamma_2/\Gamma_1 \leq 1$ (Fig. 5c). Without loss of generality, we assume that $z_3 = 0$ and $-0.5 \leq x'_1/l < 0.5$, $-0.5 \leq x'_2/l < 0.5$. We consider the equilibrium configurations [19], which satisfies the relations:

$$
\begin{aligned}
\cot\frac{\pi z_1}{l} &= \frac{\pm\alpha_0\sqrt{3\beta_0^2 - 1} - i(\alpha_0 + 2)\beta_0}{\sqrt{\alpha_0^2 + \alpha_0 + 1}} = a_1 + ib_1, \\
\cot\frac{\pi z_2}{l} &= \frac{\mp\sqrt{3\beta_0^2 - 1} - i(2\alpha_0 + 1)\beta_0}{\sqrt{\alpha_0^2 + \alpha_0 + 1}} = a_2 + ib_2.
\end{aligned}
\tag{13}
$$

Here, $\beta_0 = lU/S = \beta\Gamma/S$, $S = 0.5\Gamma\sqrt{\alpha_0^2 + \alpha_0 + 1}/(\alpha_0 + 1)$. The solution is determined by two parameters: α_0 and β_0.

For $3\beta_0^2 > 1$, different signs in Eqs. (13) correspond to the solutions which are symmetric about $x' = 0$. We choose '+' in the first equation and '−' in the second equation. Figure 6 shows the relative positions of the vortices for different parameters α_0 and β_0.

The minimum value of $\overline{u'}_{min} = -\Gamma/(2l)$ is attained for $\max(y'_1, y'_2) < y' < y'_3$, and the efficiency of energy separation is

$$
E = \frac{\Gamma}{2li_{0\infty}}\left(1 + \beta\frac{\Gamma}{l}\right),
$$

For the considered case

$$
\beta = \beta_0\frac{\sqrt{\alpha_0^2 + \alpha_0 + 1}}{2(\alpha_0 + 1)} < -\frac{1}{4}.
$$

$\beta \to -1/4$ as $\beta_0 \to -1/\sqrt{3}$ and $\alpha_0 = 1$. Thus

$$
E < \frac{\Gamma}{2li_{0\infty}}\left(1 - \frac{\Gamma}{4l}\right).
$$

9
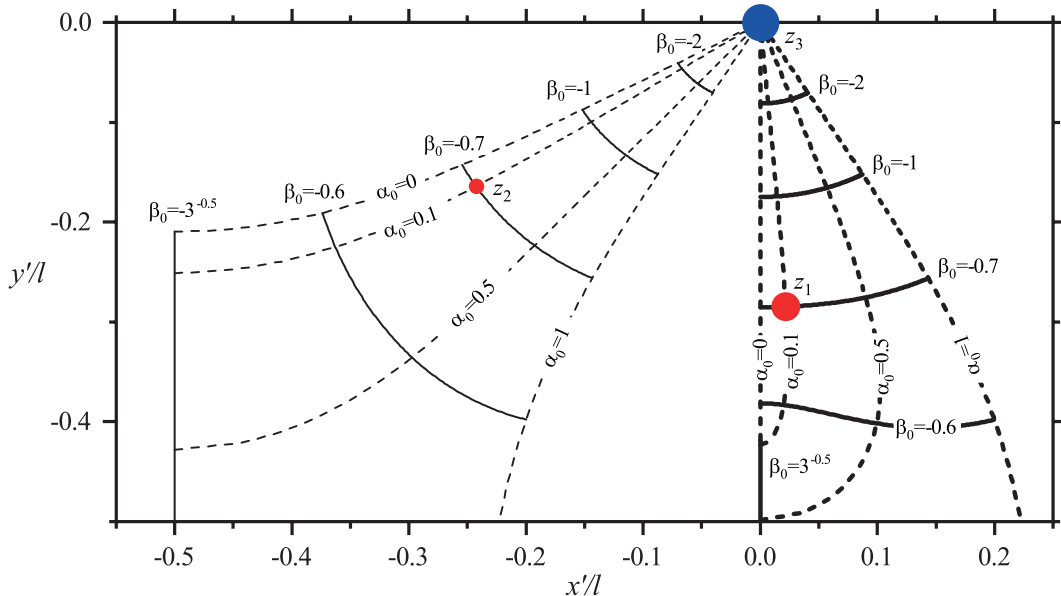
Fig. 6: The positions of the vortices for different parameters α_0 and β_0. Dashed and solid lines are the isolines of $\alpha_0 = $ const and $\beta_0 = $ const. Thick and thin lines correspond to the positions of the first and second vortices. Circles show an example of a mutual arrangement of vortices for $\alpha_0 = 0.1$ and $\beta_0 = -0.7$.

If $3\beta_0^2 \leq 1$, then the real part of the cotangent is equal to 0, therefore the possible values of x_1', x_2' are 0, $-l/2$. We consider only the case when the factor $(1 + U)$ is maximal, i.e. $U = 0$ and $\beta = 0$. The first and second vortices are located on both sides of the axis $y' = 0$ (we assume that $y_1' < 0$). Thus, the efficiency of energy separation is

$$ E = \frac{\Gamma}{2li_{0\infty}(1 + \alpha_0)}. $$

The value $\alpha_0 = 0$ corresponds to a staggered vortex street with $N = 2$ and $h = 0$. Otherwise, the scheme is less efficient.

3.2.3. N=4

We consider a symmetric 2P wake (Fig. 5d), which can be observed behind a pair of cylinders. The point vortex models for these configurations were studied in [18]. We consider the following case: $\Gamma_1 = -\Gamma_4 > 0$, $\Gamma_3 = -\Gamma_2 > 0$, $\Gamma_3 < \Gamma_1$ and $x_1' + iy_1' = x_4' - iy_4'$, $x_2' + iy_2' = x_3' - iy_3'$, $z_2 - z_1 = -l/2+ih$, $z_3-z_2 = i(H-h)$, $H > h > 0$. Thus, $\alpha_1 = -\alpha_4 > 0.25$ and $\alpha_3 = -\alpha_2 < 0.25$. Since $2(\alpha_1 + \alpha_3) = 1$, we can use only one parameter $\alpha = 2\alpha_3 < 0.5$, which is equal to parameter γ in [18].

Let us discuss the possibility of increasing the efficiency of energy separation in such configurations, as compared to the classical vortex street ($N = 2$). To be able to compare the results for $N = 2$ and $N = 4$, we assume that Γ_0 from Section 3.2.1 equals $(\Gamma_1 + \Gamma_3)/2$. As the distance H/l between two vortex streets tends to $+\infty$ ($\alpha \to 0.5$, see [18]) Γ_1 and Γ_3 tend to Γ_0, so this assumption makes sense.

The minimal value of $\overline{u'}$ is attained for $y_1' < y' < y_2'$ and $y_3' < y' < y_4'$. It equals $-\Gamma_1/l$, which is not greater than the value $-\Gamma_0/l$ for $N = 2$. Although $|\overline{u'}_{\min}|$ for $N = 4$ is greater than for $N = 2$, to make a conclusion about efficiency E one should take into account the velocities of vortices, i.e. the factor $(1 + U)$. In Fig. 7, we plotted $-1 < U < 0$ and lines $\Delta E = E_{(N=4)} - E_{(N=2)} = $ const as functions of h/l and H/l at fixed $\Gamma_0/l = 0.1$ (Fig. 7a) and 1 (Fig. 7b). These examples demonstrate the possibility to obtain ΔE of different signs. It seems particularly interesting that theoretically the creation of two vortex streets can improve the efficiency of energy separation ($\Delta E > 0$ at $\Gamma_0/l = 0.1$ in Fig. 7a).

4. Conclusions

In the present study, a clear link between the structure and intensity of a vortex street in a wake behind an oscillating cylinder and the efficiency of energy separation is demonstrated. Possible ways to improve energy separation efficiency in the wake are investigated. The study is based on both direct numerical simulations of the wake behind a transversely oscillating cylinder within the Navier-Stokes equations and the use of simplified point vortex models of vortex streets with different configurations.

It is demonstrated that the lowest values of time-averaged total enthalpy observed near the centerline of the developed wake can be significantly changed by the variation in the amplitude and frequency of forced oscillations. Pronounced changes in the area of the region of reduced total enthalpy in the wake can also be achieved. These effects are attributable to the formation of qualitatively different vortex structures in the wake. The appearance of reversed vortex pairs (with the positive vortex located

10
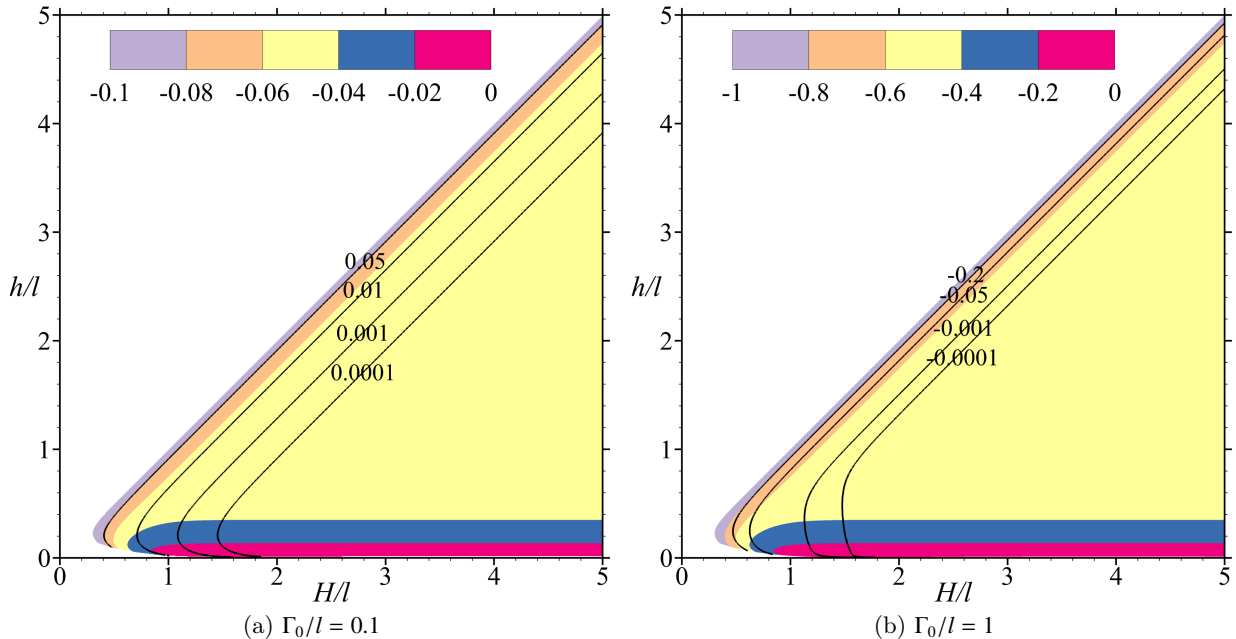
Fig. 7: The values of U (filled plot) at $N = 4$ for different mutual arrangement of vortices and the difference $\Delta Ei_{0\infty}$ (solid lines) between the efficiency of energy separation for $N = 4$ and $N = 2$. Γ_0/l is fixed and equals 0.1 (left plot) and 1 (right plot). (For interpretation of the references to color in this figure legend, the reader is referred to the web version of this article.)

above the negative one) leads to the development of regions with increased total enthalpy.

The velocity fields for different vortex street structures were approximated by point vortex models, consisting of 2, 3, and 4 infinite periodic vortex chains in the equilibrium state. Based on this approximation of the velocity fields, the distribution of total enthalpy was obtained. This approach makes it possible to easily estimate the maximum efficiency of energy separation due to pressure oscillations in the wake. For instance, in the general case of N vortex chains in the street for any fixed mutual arrangement of vortices the maximum possible efficiency is equal to $\Gamma(N-1)/(2li_{0\infty}N)$ for relative velocity of vortices equal to 0.5. The fixed arrangement here means the freezing of vortex locations (with respect to a characteristic length l), which takes place at constant normalized vortex circulations α_k and coefficient $\beta = Ul/\Gamma$.

It is demonstrated that the point vortex models can predict the energy separation efficiency well if the motion of vortex cores occurs outside the region considered. Otherwise, the results of the model can be improved using the Rankine vortices instead of the potential ones, since the main discrepancy is caused by an incorrect velocity distributions inside the vortex cores. Using the improved model for a staggered Kármán street, it was shown that the maximum efficiency of energy separation can be achieved when the transverse distance between opposite vortices is close to the vortex core diameter. This model was successfully used to simulate the effect of a significant increase in energy separation efficiency due to the natural restructuring of the vortex street in the wake behind a fixed cylinder.

For a symmetric Kármán street, the efficiency is restricted by the minimum value of efficiency for the staggered arrangement. In contrast to the staggered arrangement, the efficiency increases with the increase in the transverse distance between vortices.

The theoretical results show the possibility to increase the efficiency of energy separation by creating side-by-side Kármán vortex streets. This configuration can be formed, for example, behind a pair of cylinders placed far enough from each other.

It should be noted that all the results are obtained using two-dimensional models. For a quantitative description of energy separation in the real flows one should take into account three-dimensional effects, turbulence, and, probably, the dependence of the viscosity and thermal conduction coefficients on temperature. Nevertheless, the present study provides preliminary estimate of the influence of particular vortex structures on energy separation due to the pressure variation mechanism.

Acknowledgements

Appendix A. The Navier–Stokes equations in primitive variables

The matrices in Eq. (1) take the following form:

$$A_0 = \frac{1}{(\gamma-1)T}\begin{pmatrix} 1 & 0 & 0 & -\frac{p}{T} \\ u_1 & p & 0 & -\frac{pu_1}{T} \\ u_2 & 0 & p & -\frac{pu_2}{T} \\ \varepsilon & pu_1 & pu_2 & -\frac{p|\mathbf{u}|^2}{2T} \end{pmatrix},$$

$$A_i = \frac{1}{(\gamma-1)T}\begin{pmatrix} u_i & p\delta_{1i} & p\delta_{2i} & -\frac{pu_i}{T} \\ u_iu_1 & pu_i(1+\delta_{1i}) & pu_1\delta_{2i} & -\frac{pu_iu_1}{T} \\ u_iu_2 & pu_2\delta_{1i} & pu_i(1+\delta_{2i}) & -\frac{pu_iu_2}{T} \\ u_i\varepsilon & pu_iu_1+\delta_{1i}p\varepsilon & pu_iu_2+\delta_{2i}p\varepsilon & -\frac{pu_i|\mathbf{u}|^2}{2T} \end{pmatrix},$$

$$K_{11}=\begin{pmatrix} 0 & 0 & 0 & 0 \\ 0 & \frac{4}{3\mathrm{Re}} & 0 & 0 \\ 0 & 0 & \frac{1}{\mathrm{Re}} & 0 \\ 0 & \frac{4u_1}{3\mathrm{Re}} & \frac{u_2}{\mathrm{Re}} & \frac{\gamma}{\mathrm{PrRe}} \end{pmatrix}, K_{12}=\begin{pmatrix} 0 & 0 & 0 & 0 \\ 0 & 0 & -\frac{2}{3\mathrm{Re}} & 0 \\ 0 & \frac{1}{\mathrm{Re}} & 0 & 0 \\ 0 & \frac{u_2}{\mathrm{Re}} & -\frac{2u_1}{3\mathrm{Re}} & 0 \end{pmatrix},$$

$$K_{21}=\begin{pmatrix} 0 & 0 & 0 & 0 \\ 0 & 0 & \frac{1}{\mathrm{Re}} & 0 \\ 0 & -\frac{2}{3\mathrm{Re}} & 0 & 0 \\ 0 & -\frac{2u_2}{3\mathrm{Re}} & \frac{u_1}{\mathrm{Re}} & 0 \end{pmatrix}, K_{22}=\begin{pmatrix} 0 & 0 & 0 & 0 \\ 0 & \frac{1}{\mathrm{Re}} & 0 & 0 \\ 0 & 0 & \frac{4}{3\mathrm{Re}} & 0 \\ 0 & \frac{u_1}{\mathrm{Re}} & \frac{4u_2}{3\mathrm{Re}} & \frac{\gamma}{\mathrm{PrRe}} \end{pmatrix},$$

$$P_i = p\,(0,\delta_{1i},\delta_{2i},u_i)^*, \quad R = -\rho v_{c,t}\,(0,0,1,u_2)^*.$$

Here, $\varepsilon = T + 0.5|\mathbf{u}|^2$, δ_{ij} is Kronecker delta, $i = 1, 2, j = 1, 2$.

References

[1] M. Kurosaka, J. B. Gertz, J. E. Graham, J. R. Goodman, P. Sundaram, W. C. Riner, H. Kuroda, W. L. Hankey, Energy separation in a vortex street, Journal of Fluid Mechanics 178 (1987) 1–29. doi:10.1017/S0022112087001095.

[2] L. F. Ryan, Experiments on aerodynamic cooling, Ph.D. thesis, Swiss Federal Institute of Technology, Zurich (1951).

[3] H. Thomann, Measurements of the Recovery Temperature in the Wake of a Cylinder and of a Wedge at Mach Numbers Between 0. 5 and 3, Tech. Rep. Report 84, National Aeronautical Research Institute (FFA), Sweden (1959).

[4] E. R. G. Eckert, Cross transport of energy in fluid streams, Wärme-und Stoffübertragung 21 (2-3) (1987) 73–81. doi:10.1007/BF01377562.

[5] W. F. Ng, W. M. Chakroun, M. Kurosaka, Time-resolved measurements of total temperature and pressure in the vortex street behind a cylinder, Physics of Fluids A: Fluid Dynamics 2 (6) (1990) 971–978. doi:10.1063/1.857604.

[6] K. Kulkarni, R. Goldstein, Energy separation in the wake of a cylinder: Effect of Reynolds number and acoustic resonance, International Journal of Heat and Mass Transfer 52 (17-18) (2009) 3994–4000. doi:10.1016/j.ijheatmasstransfer.2009.03.024.

[7] A. I. Aleksyuk, A. N. Osiptsov, Direct numerical simulation of energy separation effect in the near wake behind a circular cylinder, Int. J. Heat Mass Transfer 119 (2018) 665–677. doi:10.1016/j.ijheatmasstransfer.2017.11.133.

[8] S. Eiamsa-ard, P. Promvonge, Review of Ranque–Hilsch effects in vortex tubes, Renewable and sustainable energy reviews 12 (7) (2008) 1822–1842. doi:10.1016/j.rser.2007.03.006.

[9] A. I. Leont'ev, Gas–dynamic method of energy separation of gas flows, High Temp. 35 (1) (1997) 155–157.

[10] A. I. Leontiev, A. G. Zditovets, Y. A. Vinogradov, M. M. Strongin, N. A. Kiselev, Experimental investigation of the machine-free method of temperature separation of air flows based on the energy separation effect in a compressible boundary layer, Experimental Thermal and Fluid Science 88 (2017) 202–219. doi:10.1016/j.expthermflusci.2017.05.021.

[11] E. Eckert, W. Weise, Messungen der Temperaturverteilung auf der Oberfläche schnell angeströmter unbeheizter Körper, Forschung im Ingenieurwesen 13 (6) (1942) 246–254. doi:10.1007/BF02585343.

[12] R. J. Goldstein, K. S. Kulkarni, Energy Separation in the Wake of a Cylinder, J. Heat Transfer 130 (6) (2008) 061703–061703–9. doi:10.1115/1.2891222.

[13] C. Williamson, A. Roshko, Vortex formation in the wake of an oscillating cylinder, Journal of Fluids and Structures 2 (4) (1988) 355–381. doi:10.1016/S0889-9746(88)90058-8.

[14] J. S. Leontini, B. E. Stewart, M. C. Thompson, K. Hourigan, Wake state and energy transitions of an oscillating cylinder at low Reynolds number, Physics of Fluids 18 (6) (2006) 067101. doi:10.1063/1.2204632.

[15] N. E. Kochin, I. A. Kibel, N. V. Roze, Theoretical Hydromechanics, Interscience, 1964.

[16] V. V. Meleshko, M. Y. Konstantinov, Dynamics of Vortex Structures, Naukova Dumka, Kiev, 1993.

[17] H. Aref, M. A. Stremler, On the motion of three point vortices in a periodic strip, Journal of Fluid Mechanics 314 (1996) 1–25. doi:10.1017/S0022112096000213.

[18] S. Basu, M. A. Stremler, Exploring the dynamics of '2P' wakes with reflective symmetry using point vortices, Journal of Fluid Mechanics 831 (2017) 72–100. doi:10.1017/jfm.2017.563.

[19] M. A. Stremler, Relative equilibria of singly periodic point vortex arrays, Physics of Fluids 15 (12) (2003) 3767–3775. doi:10.1063/1.1624608.

[20] A. I. Aleksyuk, V. Y. Shkadov, Analysis of three-dimensional transition mechanisms in the near wake behind a circular cylinder, European Journal of Mechanics - B/Fluids 72 (2018) 456–466. doi:10.1016/j.euromechflu.2018.07.011.

[21] A. I. Aleksyuk, V. P. Shkadova, V. Y. Shkadov, Formation, evolution, and decay of a vortex street in the wake of a streamlined body, Moscow University Mechanics Bulletin 67 (3) (2012) 53–61. doi:10.3103/S0027133012030016.

[22] H. M. Blackburn, R. D. Henderson, A study of two-dimensional flow past an oscillating cylinder, Journal of Fluid Mechanics 385 (1999) 255–286. doi:10.1017/S0022112099004309.

[23] D. G. Crowdy, V. S. Krishnamurthy, Speed of a von Kármán point vortex street in a weakly compressible fluid, Physical Review Fluids 2 (11) (2017) 114701. doi:10.1103/PhysRevFluids.2.114701.